6 th International Symposium on Solid Mechanics

Select the box to select the Mini-Symposia:

[ ] Multiaxial and Fretting Fatigue (Edgar Mamiya and Lucival Malcher);

[ ] Composite Materials (Ricardo de Medeiros);

[ ] Constitutive Models I - Plasticity and Damage (Lucival Malcher, Miguel Vaz Jr. and Edgar Mamiya);

[ ] Constitutive Models II - Viscoelastic and Viscoplastic Solids: Models and Applications (Heraldo Mattos);

[ ] Impact Engineering (Marcílio Alves);

[ ] Structural Reliability Methods and Reliability-Based Design Optimization (André Beck);

[ ] Topology Optimization of Multifunctional Materials, Fluids and Structures (Eduardo Lenz Cardoso e Emilio Carlos Nelli Silva);

[ ] Topological Derivatives: Theory and Applications (André Novotny);

[ ] X-FEM, G-FEM and Meshfree Methods (Roberto Dalledone Machado and Rodrigo Rossi);

[X] High Order Finite Elements (Marco Lúcio Bittencourt);

[ ] Nonlinear Analyses (Eduardo Campello);

[ ] Other section;

MECSOL Joinville 2017
April 26-28, 2017
Joinville, Santa Catarina, Brazil

APPLICATION OF HIGH-ORDER MINIMUM ENERGY BASES FOR TRANSIENT NON-LINEAR STRUCTURAL PROBLEMS

Jorge L. Suzuki
Department of Integrated System
School of Mechanical Engineering, University of Campinas
jluissuzuki@gmail.com

Gilberto L.V. da Costa
Department of Integrated System
School of Mechanical Engineering, University of Campinas
betogil@gmail.com

Caio F. Rodrigues
Department of Integrated System
School of Mechanical Engineering, University of Campinas
caiorodrigs@gmail.com

Marco L. Bittencourt
Department of Integrated System
School of Mechanical Engineering, University of Campinas
mlb@fem.unicamp.br

ABSTRACT

We present the application of high-order finite element bases for transient non-linear structural problems. The bases are constructed using procedures for simultaneous diagonalization of the internal modes and Schur complement of the boundary modes. The bases are obtained from nodal or modal bases constructed with Lagrange or Jacobi polynomials. Transient structural problems with large deformation and hyperelastic materials are solved using the obtained bases. Explicit and implicit time integration schemes are used. The performance of the proposed bases are compared with the results for standard nodal or modal bases.

Keywords: High-order finite element method, Minimum energy bases; Non-linear structural problems

1. INTRODUCTION

The high-order finite element method (HOFEM) corresponds to the *p*-version of the standard finite elements and the convergence of the approximate solution is achieved by increasing the polynomial order of the basis functions [1, 2]. Its application to structural analysis makes possible, for instance, to bypass problems related to mesh locking due to geometric properties and incompressibility only by increasing the polynomial order of the mesh elements [2].

The construction of appropriate basis functions is critical for the HOFEM due to the higher condition numbers of the element matrices and increasing number of non-zeros coefficients as the polynomial order increases. The use of tensor-product bases is also very important to improve the performance to calculate the element matrices and save memory space. Basis functions for structured and non-structured high-order elements are presented in [3, 4, 1, 5].

Hierarchical bases using Jacobi polynomials have been used in structural mechanics [6, 7, 8]. Particularly, simultaneous diagonalization for the internal modes and minimum energy techniques for the vertex modes were used in [8] to construct high-order bases for squares and hexahedra and applied to linear transient elastic problem. In this paper, we apply the obtained bases for transient non-linear elastic problems.

2. CONSTRUCTION OF HIGH-ORDER BASES

The one-dimensional modal standard basis (ST) of order P is defined in the local coordinate system ξ_1 as [1, 5]

$$\psi_p(\xi_1) = \begin{cases} \frac{1}{2}(1-\xi_1), & p=0, \\ \frac{1}{2}(1+\xi_1), & p=1, \\ \frac{1}{4}(1-\xi_1)(1+\xi_1)\mathscr{P}_{p-2}^{\alpha,\beta}(\xi_1), & 2 \le p \le P, \end{cases} . \tag{1}$$

where $\mathscr{P}_p^{\alpha,\beta}(\xi_1)$ indicates the Jacobi orthogonal polynomials of order p and weights (α,β). This is a hierarchical basis because the set of functions of order P is included in the set of functions of order $P+1$. The vertex or boundary functions correspond to the indices $p=0$ and $p=1$; the internal functions are obtained for $2 \le p \le P$. The modal shape functions are related to the elemental topological entities: vertices, edges, faces and volumes.

The local coefficients of the one-dimensional mass and stiffness matrices are respectively given by

$$M_{pq} = \int_{-1}^{1} \psi_p(\xi_1)\psi_q(\xi_1)d\xi_1, \tag{2}$$

$$K_{pq} = \int_{-1}^{1} \psi_{p,\xi_1}(\xi_1)\psi_{q,\xi_1}(\xi_1)d\xi_1, \tag{3}$$

where $0 \le p,q \le P$ and ψ_{p,ξ_1} is the derivative of ψ_p with respect to ξ_1. Fig. 1 illustrates the sparsity profiles of the mass and stiffness matrices for $P=10$ and $\alpha=\beta=1$.

We can partition the previous mass and stiffness element matrices in terms of the vertex and internal modes as

$$[M] = \begin{bmatrix} [M_{vv}] & [M_{vi}] \\ [M_{vi}]^T & [M_{ii}] \end{bmatrix} \quad \text{and} \quad [K] = \begin{bmatrix} [K_{vv}] & [K_{vi}] \\ [K_{vi}]^T & [K_{ii}] \end{bmatrix}. \tag{4}$$

The internal modes for the basis given in Eq.(1) will be transformed according to [9, 10] as:

$$\varphi_p(\xi_1) = \sum_{q=2}^{P} y_{pq}\psi_q(\xi_1). \tag{5}$$

The coefficients y_{pq} are entries of matrix $[Y]$ such that the internal modes of the new mass $\left[M_{ii}^{'}\right]$ and stiffness $\left[K_{ii}^{'}\right]$ matrices related to the internal modes are given respectively by

$$\left[M_{ii}^{'}\right] = [Y]\,[M_{ii}]\,[Y]^T \quad \text{and} \quad \left[K_{ii}^{'}\right] = [Y]\,[K_{ii}]\,[Y]^T. \tag{6}$$

The standard internal mass matrix $[M_{ii}]$ can be made diagonal using

$$[X]^T [M_{ii}] [X] = [\Lambda_M], \tag{7}$$

where $[X]$ is the eigenvector matrix of $[M_{ii}]$ and $[\Lambda_M]$ is the diagonal matrix with the eigenvalues of $[M_{ii}]$. Based on that, we can define the matrix

$$[L] = \left([X] \left[\Lambda_M^{-\frac{1}{2}} \right] \right)^T [K_{ii}] \left([X] \left[\Lambda_M^{-\frac{1}{2}} \right] \right), \tag{8}$$

which is also symmetric and positive-definite and can be diagonalized as

$$[Z]^T [L] [Z] = [\Lambda_S], \tag{9}$$

in which $[Z]$ denotes the matrix of the eigenvectors and $[\Lambda_S]$ represents the diagonal matrix with eigenvalues of $[L]$. Therefore, $[Y]$ is then defined as

$$[Y] = \left([X] \left[\Lambda_M^{-\frac{1}{2}} \right] [Z] \left[\Lambda_S^{-\frac{k}{2}} \right] \right)^T, \tag{10}$$

where $k \in [0,1]$ is a parameter that influences the condition number of the matrices related to the internal modes.

Substituting $[Y]$ from (10) into (6) yields

$$\left[M_{ii}^{'} \right] = [Y] [M_{ii}] [Y]^T = \left[\Lambda_S^{-k} \right] \text{ and } \left[K_{ii}^{'} \right] = [Y] [K_{ii}] [Y]^T = \left[\Lambda_S^{1-k} \right]. \tag{11}$$

For $k = 0$, the internal block of the mass matrix is the identity matrix and the condition number is 1 for any polynomial order. Analogously for the stiffness matrix with $k = 1$. The same condition number of the internal mass and stiffness matrices is obtained for $k = \frac{1}{2}$.

The construction of minimum energy bases is equivalent to apply the Schur complement for the vertex modes. Therefore, the minimum energy extension of the standard basis is computed as:

$$\varphi_k = \psi_k^v - \sum_{j=2}^{P} \alpha_{kj} \psi_j^i, \;\; k = 0, 1, \tag{12}$$

where the coefficients α_{kj} are defined according to an appropriate norm. For instance, α_{kj}^M denotes the coefficients using for the L_2 (or mass) norm, which are uniquely determined as [8]

$$\langle \psi_k^v, \psi_l^i \rangle_{L_2} - \sum_{j=2}^{P} \alpha_{kj}^M \langle \psi_j^i, \psi_l^i \rangle_{L_2} = 0, \;\; \forall \psi_l^i \in V^i, \tag{13}$$

which results in the following matrix for the coefficients α_{kj}^M:

$$\left[\alpha^M \right] = [M_{vi}] [M_{ii}]^{-1}. \tag{14}$$

We consider the simultaneous diagonalization (SD) of the internal blocks of the mass and stiffness matrices to construct the one-dimensional internal modes and the minimum energy (ME) orthogonalization for the boundary modes. This allows us to generalize the orthogonalization procedure for the boundary modes based on the choice of the appropriate norm according to the considered problem. The obtained bases are labeled SDME. Specifically, when using $\left[\alpha^M \right]$ we denote the basis as SDME-M.

Figure 1 shows the sparsity patterns of the local one-dimensional mass and stiffness matrices for the standard basis and the SDME basis with $\left[\alpha^M\right]$.

We can also write Eq.(13) in terms of the energy norm as:

$$\langle \psi_k^v, \psi_l^i \rangle_E - \sum_{j=2}^{P} \alpha_{kj}^K \langle \psi_j^i, \psi_l^i \rangle_E = 0, \ \ \forall \psi_l^i \in V^i, \tag{15}$$

which results in the following matrix for the coefficients α_{kj}^K [8]:

$$\left[\alpha^K\right] = \left[K_{vi}\right] \left[K_{ii}\right]^{-1}. \tag{16}$$

We observe that the matrix $[\alpha]$ influences the coupling blocks $[M_{vi}], [K_{vi}]$ of the mass and stiffness matrices. For $\left[\alpha^M\right]$, the basis does not decouple internal and boundary modes of the one-dimensional stiffness matrix. However, the one-dimensional mass matrix has the internal and boundary blocks uncoupled.

When using an implicit Newmark scheme for time integration, an effective stiffness matrix $[\hat{K}]$ of the following form arises:

$$[\hat{K}] = [K] + a_0 [M], \tag{17}$$

where $a_0 = \frac{1}{4\Delta t^2}$ and Δt is the time increment. For the construction of the one-dimensional basis, we can associate the coefficient a_0 with a parameter *lambda*, such that:

$$[\hat{K}] = [K] + \lambda [M], \tag{18}$$

The matrix $[\hat{K}]$ can be expressed in terms of vertex and internal modes. For $\lambda = 1$ and considering the minimum energy procedure for the energy norm of function u given by $\|u\|_E^2 = \langle u', u' \rangle_{L_2} + \lambda \langle u, u \rangle_{L_2}$, we obtain the following coefficients for the matrix $[\alpha]^{\hat{K}}$ with $\lambda = 1$:

$$\left[\alpha^{\hat{K}}\right] = \left[\hat{K}_{vi}\right] \left[\hat{K}_{ii}\right]^{-1}. \tag{19}$$

The boundary and internal blocks are uncoupled for $[\hat{K}]$ as illustrated in Fig.1. The obtained basis is labeled as SDME-H.

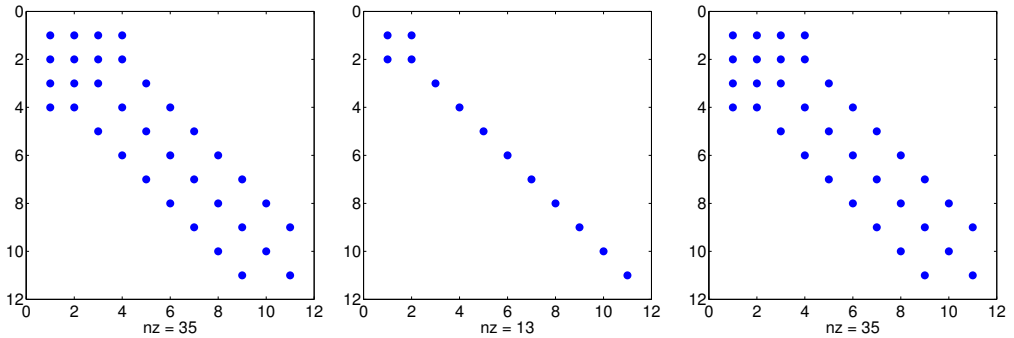

(a) $[M]$, ST basis. (b) $[K]$, ST basis. (c) $\left[\hat{K}\right]$, ST basis.

(d) $[M]$, SDME basis. (e) $[K]$, SDME basis. (f) $\left[\hat{K}\right]$, SDME basis.

Figure 1: Sparsity patterns of the mass, stiffness and effective stiffness one-dimensional local matrices for $P = 10$ using the standard basis (ST) and the SDME basis with $\lambda = 1$.

3. SDME BASES FOR QUADRILATERALS AND HEXAHEDRA

The shape functions for quadrilaterals and hexahedra are obtained using the tensor product of the previous one-dimensional functions respectively in the local coordinate systems $\xi_1 \times \xi_2$ and $\xi_1 \times \xi_2 \times \xi_3$ [1, 5, 2]:

$$N_i(\xi_1,\xi_2) = \varphi_p(\xi_1)\varphi_q(\xi_2) \ \ (0 \le p,q \le P), \tag{20}$$

$$N_i(\xi_1,\xi_2,\xi_3) = \varphi_p(\xi_1)\varphi_q(\xi_2)\varphi_r(\xi_3) \ \ (0 \le p,q,r \le P), \tag{21}$$

where p, q and r are tensor product indices associated with the topological entities of the element; P the polynomial order in directions ξ_1, ξ_2 and ξ_3; $i = 1,\ldots,(P+1)^2$ for squares and $i = 1,\ldots,(P+1)^3$ for hexahedra. The SDME bases are conforming and continuous on the element boundaries.

One important aspect to achieve CPU performance and reduce memory requirements is to take advantage of the tensor product nature of the shape functions and integration points. Therefore, we use only the values of the shape functions calculated at the coordinates of one-dimensional integration points when calculating higher dimensional operators. This feature will be illustrated for the tangent stiffness matrix of quadrilaterals for non-linear elastic problems.

In Einstein's notation, the tangent stiffness matrix in a total Lagrangian formulation for a given two-dimensional element is given by:

$$(K_T^e)_{st}(i,j) = \frac{1}{4}\sum_{p,q,k,l=1}^{2}\int_{\Omega^e}\mathscr{C}_{pqkl}[N_{s,p}N_{t,k}F_{iq}F_{jl} + N_{s,p}N_{t,l}F_{iq}F_{jk} + N_{s,q}N_{t,k}F_{ip}F_{jl} + N_{s,q}N_{t,l}F_{ip}F_{jk}]\,d\Omega^e$$

$$+ \ \delta_{ij}\sum_{p,q=1}^{2}\int_{\Omega^e}S_{pq}N_{s,p}N_{t,q}\,d\Omega^e,$$

with $i, j = 1,2$ and $s,t = 1,...,(P+1)^2$, where P is the polynomial order. The terms $N_{s,p}$ and $N_{t,p}$ are the global derivatives of the shape functions in terms of the initial coordinates X_p. The term F is the deformation gradient, $\mathscr{C}_{pqkl}$ is the fourth-order constitutive tensor and S_{pq} is the second-order stress tensor. Therefore, the implementation of the tangent matrix consists on expanding the above expression after the substitution of Eq.(20) and its partial derivatives. The computation of the global derivatives is performed the same way as the stiffness matrix for linear problems, where the terms involving the one-dimensional mass, stiffness and combines matrices arise [8].

The internal force vector is given by

$$(R^e)(i) = -\frac{1}{2}\sum_{k,l=1}^{2}\int_{\Omega^e} S_{kl}\left(N_{s,k}F_{il} + F_{ik}N_{s,l}\right)\, d\Omega^e.$$

Although the representation in Einstein's notation is more compact, to derive the tangent matrix we started with the conventional matrix product given by:

$$[\mathbf{K}_T^e] = \int_{\Omega^e}[\mathbf{B}_{L,s}]^T[\mathbf{D}][\mathbf{B}_{L,t}]\, d\Omega^e + \int_{\Omega^e}[\mathbf{B}_{\sigma,s}]^T[\mathbf{T}][\mathbf{B}_{\sigma,t}]\, d\Omega^e, \tag{22}$$

with $[\mathbf{D}]$ being the constitutive matrix in Voigt notation and $[\mathbf{T}] = \mathbf{S}\otimes\mathbf{S}$. The term of the tangent stiffness for $i = j = 1$ after some algebraic manipulation is given by

$$\begin{aligned}(K_T^e)_{st}(1,1) &= \left[\mathscr{C}_{1111}F_{11}F_{11} + 2\mathscr{C}_{1112}F_{11}F_{12} + \mathscr{C}_{1212}F_{12}F_{12}\right] N_{s,1}N_{t,1} \\ &+ \left[\mathscr{C}_{1212}F_{11}F_{11} + 2\mathscr{C}_{1222}F_{11}F_{12} + \mathscr{C}_{1212}F_{12}F_{12}\right] N_{s,2}N_{t,2} \\ &+ \left[\mathscr{C}_{1112}F_{11}F_{11} + (\mathscr{C}_{1122} + \mathscr{C}_{1212})F_{11}F_{12} + \mathscr{C}_{1222}F_{12}F_{12}\right] (N_{s,1}N_{t,2} + N_{s,2}N_{t,1})\end{aligned}$$

A final expression in terms of the one-dimensional mass, stiffness and combined matrices can be obtained by replacing the global derivatives in the above equation.

This procedure is labeled 1D matrices and more details may be found in [8].

4. NON-LINEAR TRANSIENT PROBLEMS

In this section we introduce the equation for conservation of linear momentum in discrete form, and show the explicit central difference and implicit Newmark time-integration schemes employed, with the respective forms after applying the Schur complement to condense the internal modes.

4.1 EXPLICIT TIME INTEGRATION

We consider the equation of motion in discrete form for the current time t_n, neglecting damping effects, for non-linear elastic problems as:

$$\mathbf{M}\mathbf{a}_n + \mathbf{R}(\mathbf{u}_n) = \mathbf{P}_n, \tag{23}$$

with $\mathbf{M}$ denoting the global mass matrix in the reference configuration, $\mathbf{a}_n$ the global acceleration vector, $\mathbf{R}(\mathbf{u}_n)$ the global internal force vector, and $\mathbf{P}_n$ the global external load vector. The velocities $\mathbf{v}_n$ and accelerations $\mathbf{a}_n$ can be approximated using the central-difference schemes in the following way:

$$\mathbf{v}_n = \frac{\mathbf{u}_{n+1} - \mathbf{u}_{n-1}}{2\Delta t}, \qquad \mathbf{a}_n = \frac{\mathbf{u}_{n+1} - 2\mathbf{u}_n + \mathbf{u}_{n-1}}{\Delta t^2}, \tag{24}$$

where Δt represents the time increment. Substituting the accelerations $\mathbf{a}_n$ from Eq.(24) into Eq.(40), and rearranging the terms, we obtain

$$\hat{\mathbf{M}}\mathbf{u}_{n+1} = \psi_n + \hat{\mathbf{M}}(2\mathbf{u}_n - \mathbf{u}_{n-1}), \tag{25}$$

with,

$$\hat{\mathbf{M}} = \frac{1}{\Delta t^2}\mathbf{M}, \tag{26}$$

$$\psi_n = \mathbf{P}_n - \mathbf{R}\left(\mathbf{u}_n\right). \tag{27}$$

Therefore, we must solve Eq.(25) to determine the displacements at time t_{n+1}. Considering initial conditions for the displacements and velocities ($\mathbf{u}_0$, $\mathbf{v}_0$ known), the initial condition for the acceleration can be obtained by setting $t = t_0$ in Eq .(40), thus

$$\mathbf{a}_0 = \mathbf{M}^{-1}\psi_0. \tag{28}$$

The displacement for time $t = t_{-1}$ can be obtained with Eq.(24), and is given by

$$\mathbf{u}_{-1} = \mathbf{u}_0 - \Delta t\mathbf{v}_0 + \frac{\Delta t^2}{2}\mathbf{a}_0. \tag{29}$$

We can express Eq.(25) in terms of the boundary and internal modes in the following form:

$$\begin{bmatrix}\hat{\mathbf{M}}_{bb} & \hat{\mathbf{M}}_{bi}\\ \hat{\mathbf{M}}_{bi}^T & \hat{\mathbf{M}}_{ii}\end{bmatrix}\begin{bmatrix}\mathbf{u}_b\\ \mathbf{u}_i\end{bmatrix}_{n+1} = \begin{bmatrix}\psi_b\\ \psi_i\end{bmatrix}_n + \begin{bmatrix}\hat{\mathbf{M}}_{bb} & \hat{\mathbf{M}}_{bi}\\ \hat{\mathbf{M}}_{bi}^T & \hat{\mathbf{M}}_{ii}\end{bmatrix}\begin{bmatrix}\mathbf{u}_b^*\\ \mathbf{u}_i^*\end{bmatrix}, \tag{30}$$

with

$$\begin{bmatrix}\mathbf{u}_b^*\\ \mathbf{u}_i^*\end{bmatrix} = \begin{bmatrix}2\mathbf{u}_b\\ 2\mathbf{u}_i\end{bmatrix}_n - \begin{bmatrix}\mathbf{u}_b\\ \mathbf{u}_i\end{bmatrix}_{n-1} \tag{31}$$

Expanding Eq.(30) in terms of the boundary, and dropping the subscripts for time (but keeping in mind that our unknowns are $\mathbf{u}_b$ and $\mathbf{u}_i$), we obtain the following equations:

$$\hat{\mathbf{M}}_{bb}\mathbf{u}_b + \hat{\mathbf{M}}_{bi}\mathbf{u}_i = \psi_b + \hat{\mathbf{M}}_{bb}\mathbf{u}_b^* + \hat{\mathbf{M}}_{bi}\mathbf{u}_i^* \tag{32}$$

$$\hat{\mathbf{M}}_{bi}^T\mathbf{u}_b + \hat{\mathbf{M}}_{ii}\mathbf{u}_i = \psi_i + \hat{\mathbf{M}}_{bi}^T\mathbf{u}_b^* + \hat{\mathbf{M}}_{ii}\mathbf{u}_i^*. \tag{33}$$

Multiplying Eq.(33) by $\hat{\mathbf{M}}_{ii}^{-1}$ and solving for $\mathbf{u}_i$, we obtain

$$\mathbf{u}_i = \mathbf{u}_i^* + \hat{\mathbf{M}}_{ii}^{-1}\left(\psi_i - \hat{\mathbf{M}}_{bi}^T\mathbf{u}_b + \hat{\mathbf{M}}_{bi}^T\mathbf{u}_b^*\right). \tag{34}$$

Substituting the above equation into Eq.(32), and rearranging the terms, we have

$$\left(\hat{\mathbf{M}}_{bb} - \hat{\mathbf{M}}_{bi}\hat{\mathbf{M}}_i^{-1}\hat{\mathbf{M}}_{bi}^T\right)\mathbf{u}_b = \psi_b - \hat{\mathbf{M}}_{bi}\hat{\mathbf{M}}_i^{-1}\psi_i + \left(\hat{\mathbf{M}}_{bb} - \hat{\mathbf{M}}_{bi}\hat{\mathbf{M}}_i^{-1}\hat{\mathbf{M}}_{bi}^T\right)\mathbf{u}_b^*. \tag{35}$$

We can represent the above equation as

$$\hat{\mathbf{M}}_b^{sc}\mathbf{u}_b = \psi_b^{sc} + \hat{\mathbf{M}}_b^{sc}\mathbf{u}_b^*, \tag{36}$$

where

$$\hat{\mathbf{M}}_b^{sc} = \hat{\mathbf{M}}_{bb} - \hat{\mathbf{M}}_{bi}\hat{\mathbf{M}}_i^{-1}\hat{\mathbf{M}}_{bi}^T, \tag{37}$$

$$\psi_b^{sc} = \psi_b - \hat{\mathbf{M}}_{bi}\hat{\mathbf{M}}_i^{-1}\psi_i. \tag{38}$$

We can solve Eq.36 to obtain

$$\mathbf{u}_b = \hat{\mathbf{M}}_b^{sc^{-1}}\psi_b^{sc} + \mathbf{u}_b^*. \tag{39}$$

Therefore, we perform the Schur complement on $\hat{\mathbf{M}}_b$ and ψ_b, calculate the boundary modes from Eq.(39) and recover the internal modes using Eq.(34).

4.2 IMPLICIT TIME INTEGRATION (NEWMARK)

We consider the equilibrium equation for the current time step $n+1$:

$$\mathbf{M}\mathbf{a}_{n+1} + \mathbf{R}_{n+1} = \mathbf{P}_{n+1}, \tag{40}$$

where we denote $\mathbf{M}$ as the global mass matrix, $\mathbf{R}_{n+1}$ as the global internal force vector dependent of the updated configuration with coordinates $\mathbf{x}_{n+1}$, which in turn depend on the displacements $\mathbf{u}_{n+1}$. The term $\mathbf{P}_{n+1}$ represents the global external nodal force vector. The terms $\mathbf{a}_{n+1}$ and $\mathbf{v}_{n+1}$ respectively denote the global acceleration and velocity vectors.

We define the following residual force vector ψ_{n+1}, which assumes zero value when the system is at equilibrium at time step $n+1$:

$$\psi_{n+1} = \mathbf{M}\mathbf{a}_{n+1} + \mathbf{R}_{n+1} - \mathbf{P}_{n+1} = \mathbf{0}. \tag{41}$$

The following approximations for the velocity and accelerations are used by the Newmark scheme:

$$\mathbf{a}_{n+1} = b_1\left(\mathbf{u}_{n+1} - \mathbf{u}_n\right) - b_2\mathbf{v}_n - b_3\mathbf{a}_n \tag{42}$$

$$\mathbf{v}_{n+1} = b_4\left(\mathbf{u}_{n+1} - \mathbf{u}_n\right) - b_5\mathbf{v}_n - b_6\mathbf{a}_n, \tag{43}$$

with the following coefficients,

$$b_1 = \frac{1}{g_1\Delta t^2}, \quad b_2 = \frac{1}{g_1\Delta t}, \quad b_3 = \frac{1-2g_1}{2g_1}$$
$$b_4 = \frac{g_2}{g_1\Delta t^2},\ b_5 = \left(1 - \frac{g_2}{g_1}\right),\ b_6 = \left(1 - \frac{g_2}{2g_1}\right)\Delta t.$$

It is usual to choose $g_1 = 0.5$ to obtain quadratic convergence in time and $g_2 = 0.25$ for unconditional stability. Substituting Eq.42 in Eq.41, we obtain:

$$\psi_{n+1} = \mathbf{M}\left[b_1\left(\mathbf{u}_{n+1} - \mathbf{u}_n\right) - b_2\mathbf{v}_n - b_3\mathbf{a}_n\right] + \mathbf{R}_{n+1} - \mathbf{P}_{n+1} = \mathbf{0}, \tag{44}$$

The equilibrium system, Eq.(44) is linearized for the employment of Newton-Raphson method using incremental global displacements, defined as

$$\mathbf{u}_{n+1}^{k+1} = \mathbf{u}_{n+1}^{k} + \Delta\mathbf{u}. \tag{45}$$

Accordingly, the updated global coordinates are given by

$$\mathbf{x}_{n+1}^{k+1} = \mathbf{x}_n + \mathbf{u}_{n+1}^{k+1}, \tag{46}$$

where the superscript $k+1$ refers to the current iteration of the Newton's method.

The linearized form of Eq.44 in the direction of a displacement increment $\Delta\mathbf{u}$ is given by the following system of equations:

$$\left[b_1\mathbf{M} + \mathbf{K}_{T_{n+1}}^{k}\right]\Delta\mathbf{u} = -\mathbf{M}\left[b_1(\mathbf{u}_{n+1}^{k} - \mathbf{u}_n) - b_2\mathbf{v}_n - b_3\mathbf{a}_n\right] - \mathbf{R}_{n+1}^{k} + \mathbf{P}_{n+1}. \tag{47}$$

The terms $\mathbf{u}_n$, $\mathbf{v}_n$, $\mathbf{a}_n$ are obtained from the last converged time step n. The term $\mathbf{K}_T$ is the tangent stiffness matrix and is updated at each iteration k along with the internal force vector.

Now we consider the application of the Schur complement for the system described by Eq.(47). We will drop the scripts $n+1$ and k for simplicity. Consider Eq.(47) rewritten in the following form:

$$\hat{\mathbf{K}}\Delta u = \psi, \tag{48}$$

where $\hat{\mathbf{K}}$ denotes the effective tangent stiffness matrix

$$\hat{\mathbf{K}} = b_1\mathbf{M} + \mathbf{K}^T, \tag{49}$$

and ψ represents the residual force vector

$$\psi = -\mathbf{M}\mathbf{a} - \mathbf{R}^k_{n+1} + \mathbf{P}_{n+1}. \tag{50}$$

Different from the explicit method, we apply the Schur complement directly on the equivalent system Eq.(48), since we work with an equivalent global matrix in this case. Writing the system in matrix form with boundary, internal and coupled blocks, we obtain:

$$\begin{bmatrix} \hat{\mathbf{K}}_{bb} & \hat{\mathbf{K}}_{bi} \\ \hat{\mathbf{K}}^T_{bi} & \hat{\mathbf{K}}_{ii} \end{bmatrix} \begin{bmatrix} \Delta\mathbf{u}_b \\ \Delta\mathbf{u}_i \end{bmatrix} = \begin{bmatrix} \psi_b \\ \psi_i \end{bmatrix}, \tag{51}$$

where, after applying the Schur complement, we have

$$\left(\hat{\mathbf{K}}_{bb} - \hat{\mathbf{K}}_{bi}\hat{\mathbf{K}}^{-1}_{ii}\hat{\mathbf{K}}^T_{bi}\right)\Delta\mathbf{u}_b = \left(\psi_b - \hat{\mathbf{K}}_{bi}\hat{\mathbf{K}}^{-1}_{ii}\psi_i\right), \tag{52}$$

$$\Delta\mathbf{u}_i = \hat{\mathbf{K}}^{-1}_{ii}\left(\psi_i - \hat{\mathbf{K}}^T_{bi}\Delta\mathbf{u}_b\right). \tag{53}$$

5. NUMERICAL RESULTS

In this section we analyze the performance of the presented SDME bases compared to the standard (ST) Jacobi basis in terms of number of iterations for linear system solution using conjugate gradient scheme, and the computational time for solution of each time step. For this purpose, we use fabricated solutions that correspond to large displacements and strains. Static and transient simulations are performed, considering a hyperelastic Neo-Hooke material. We also measure the performance of the 1D matrices procedure to calculate the tangent stiffness for the static and implicit dynamic cases.

5.1 STATIC NON-LINEAR PROBLEM WITH LARGE STRAIN

To verify the performance of the standard and minimum energy bases, we consider the cube domain with coordinates $0 \leq x,y,z \leq 1$ discretized using 8 hexahedra and the fabricated solution:

$$u_x = 1.9\sin(x) - x, \quad u_y = 0, \quad u_z = 0. \tag{54}$$

The Young's modulus and Poisson ratio are $E = 1000\,Pa$ and $\nu = 0.3$.

We consider the ST, SDME-M and SDME-H ($\lambda = 100$) bases with $k = 0.5$. We consider the average number of iterations of the conjugate gradient method with diagonal preconditioner (CGD) and time (for linear system solution) per Newton-Raphson iteration. The CGD tolerance is 10^{-12} and Newton solver tolerance of 10^{-8}. We perform the Schur complement on the tangent stiffness matrix and residual (out-of-balance) force vector. We are also considering isoparametric mapping.

From Table 1, we observe that the standard basis require 7.85 times more iterations when compared to the SDME-M basis for $P = 8$. The same ratio is obtained for the average time in Table 2. The use of the SDME-H basis provided better performance than the SDME-M basis for $P < 8$. The results for the convergence analysis showed no issues for the SDME bases.

Degree	Number of DOFs	Average number of CGD iterations		
		ST	SDME-M	SDME-H
2	300	75.8	43.2	41.2
4	1944	249.4	67.2	57
6	6084	444.4	81.8	64
8	13872	660	84	95

Table 1: Average number of CGD iterations per Newton iteration, total of 5 Newton iterations for convergence. We observe for this case, that the best results are achieved for the SDME-M basis.

Degree	Number of DOFs	Average time for CGD solution [s]		
		ST	SDME-M	SDME-H
2	300	0.0042	0.0024	0.0023
4	1944	0.2230	0.0598	0.0501
6	6084	2.0236	0.3760	0.2464
8	13872	9.7028	1.2363	1.4031

Table 2: Average time for CGD solution.

The same analysis was performed using the conjugate gradient method with the Gauss-Seidel preconditioner (CGGS). The results are presented in Tables 3 and 4, showing a better performance of the SDME-H basis for all polynomial orders. The L^2-error norm for each displacement component is given in Table 5.

Degree	Number of DOFs	Average number of CGGS iterations		
		ST	SDME-M	SDME-H
2	300	61.2	49.6	47.8
4	1944	132.0	60.4	52.6
6	6084	218.2	66.4	51.6
8	13872	313.0	65.4	56.6

Table 3: Average number of CGGS iterations per Newton iteration, total of 5 Newton iterations for convergence. Notice that using this preconditioner for the CG scheme, we achieved a better performance for the SDME-H basis.

Degree	Number of DOFs	Average time for CGGS solution [s]		
		ST	SDME-M	SDME-H
2	300	0.0031	0.0026	0.0023
4	1944	0.1037	0.0496	0.0419
6	6084	0.8952	0.2856	0.2389
8	13872	4.2829	0.9190	0.7569

Table 4: Average time for CGGS solution.

Degree	Number of DOFs	L^2 error		
		u_x	u_y	u_z
2	300	1.10e-3	1.98e-4	1.98e-4
4	1944	7.23e-7	1.12e-7	1.12e-7
6	6084	5.69e-9	7.18e-10	7.18e-10
8	13872	1.00e-10	1.06e-11	1.06e-11
10	26460	1.94e-12	1.79e-13	1.79e-13

Table 5: L^2 error using all bases.

5.2 CALCULATION OF ELEMENT MATRICES

We also computed the time to calculate the element matrices from the tests in the previous section, as well as the error of the analysis.

For quadrilateral elements, we computed the element tangent matrix time and performed the convergence analysis using a mesh with 4 quadrilaterals. Table 6 shows the speedup obtained by the use of the tensor product of the one-dimensional matrices compared to the standard procedure. An approximate speedup of 2 is observed for the entire range of polynomial degrees used.

Degree	Standard	1D matrices	Speedup
2	0.00004	0.00001	2.10526
4	0.00039	0.00018	2.20000
6	0.00265	0.00130	2.03678
8	0.00947	0.00511	1.85183
10	0.03220	0.01595	2.01880
12	0.08662	0.04295	2.01678
14	0.22325	0.09956	2.24217

Table 6: Speedup to calculate the element tangent stiffness matrices for quadrilaterals.

The approximation error is presented in Table 7 for the mesh with 4 quadrilaterals.

Degree	Number of DOFs	L^2 error - standard		L^2 error - 1D matrices	
		u_x	u_y	u_x	u_y
2	40	1.07E-003	2.28E-004	1.19E-003	2.57E-004
4	144	7.13E-007	1.20E-007	7.52E-007	1.55E-007
6	312	5.57E-009	7.49E-010	5.27E-009	1.02E-009
8	544	9.87E-011	1.09E-011	9.24E-011	1.55E-011
10	840	1.92E-012	1.83E-013	1.78E-012	2.73E-013
12	1200	3.93E-014	3.50E-015	3.62E-014	5.36E-015
14	1624	1.14E-015	4.09E-016	1.53E-015	5.03E-016

Table 7: L^2 error using all bases with the 1D matrices procedure, quadrilaterals.

For hexahedra, we computed the element tangent matrix time using a single element mesh, and the convergence analysis was performed using a mesh with 8 hexahedra. Table 8 shows the speedup

obtained by the use of the tensor product of the one-dimensional matrices compared to the standard procedure. An approximate speedup of 2 was also observed for the entire range of polynomial degrees used.

Degree	Standard	1D matrices	Speedup
2	0.0021	0.0008	2.345
4	0.1390	0.0741	1.874
6	3.1163	1.5123	2.061
8	29.570	14.208	2.081
10	179.09	86.603	2.068
12	849.35	378.48	2.244
14	3013.45	1433.03	2.103

Table 8: Speedup to calculate the element tangent stiffness matrices for hexahedra.

The approximation error is presented in Table 9 for the mesh with 8 hexahedra.

Degree	Number of DOFs	L^2 error		
		u_x	u_y	u_z
2	300	1.10e-3	1.68e-4	1.83e-4
4	1944	6.95e-7	1.33e-7	1.22e-7
6	6084	4.51e-9	7.99e-10	8.51e-10
8	13872	8.16e-11	1.21e-11	1.22e-11
10	26460	1.60e-12	2.56e-13	2.32e-13
12	45000	3.16e-14	4.22e-15	4.59e-15

Table 9: L^2 error using all bases with the 1D matrices procedure, hexahedra.

5.3 TRANSIENT NON-LINEAR PROBLEMS WITH LARGE STRAIN

5.3.1 Explicit time integration

We consider a solid with a compressible Neo-Hookean material and the cubic spatial domain $0 \leq x,y,x \leq 1$ discretized using 8 hexahedra. The time domain is $t = [0, 0.25]\,s$. We use the following fabricated solution:

$$u_x = \sin\left(\frac{\pi}{2}x\right)\sin(2\pi t), \quad u_y = 0, \quad u_z = 0, \tag{55}$$

which gives $u_x = 1.0$ for $x = 1.0$ and $t = 0.25\,s$. The material properties considered are $E = 1000\,Pa$, $\nu = 0.3$ and $\rho = 1\,kg/m^3$. We applied homogeneous Dirichlet boundary conditions in all directions of the face with coordinate $x = 0$.

We used a rough estimate of the number of time steps using the CFL condition as [**?**]:

$$\Delta t \leq \delta \frac{h}{c_L}, \tag{56}$$

where h represents the element length (considered as the edge length in the initial configuration for this problem), δ denotes a constant in the range $0.2 < \delta < 0.9$, and

$$c_L = \frac{3K(1-\nu)}{\rho(1+\nu)}, \qquad K = \frac{E}{3(1-2\nu)}. \tag{57}$$

Considering the given material properties and $\delta = 0.85$, we obtained $\Delta t = 3.33 \times 10^{-4}$ and $N \approx 800$ times steps for the analysis for a single load step.

We used the 1D matrices procedure of Section 3to calculate the element operators, Schur complement on the effective mass matrix and performed a convergence analysis in space by increasing the polynomial order. The results are given in Table 10 for the ST basis and in Table 11 for the SDME-M basis. From Table 11, we observe a spectral convergence rate for polynomial order up to 6 and then a linear decay to order 8. We remark that the loss of spectral convergence in degree 8 can be associated with the time discretization.

Degree	Number of DOFs	L^2 error		
		u_x	u_y	u_z
2	276	2.08e-3	2.45e-4	2.26e-4
4	1246	3.38e-6	5.16e-7	5.61e-7
6	3084	4.21e-8	6.09e-9	5.76e-9

Table 10: L^2 error using the 1D-Matrices procedure, ST basis, hexahedra.

Degree	Number of DOFs	L^2 error		
		u_x	u_y	u_z
2	276	2.09e-3	2.53e-4	2.34e-4
4	1246	3.36e-6	5.06e-7	5.51e-7
6	3084	4.21e-8	6.08e-9	5.76e-9
8	5640	2.64e-8	2.01e-9	2.01e-9

Table 11: L^2 error using the 1D-Matrices procedure, SDME-M basis, hexahedra.

We also compared the performance of the SDME-M and ST bases, with the average time and average number of iterations using the conjugate gradient method with Gauss-Seidel preconditioner with tolerance of 10^{-12} to solve the linear system of equations. The results for the number of iterations are presented in Table 12. The performance results in terms of computational time per time step Δt are presented in Table 13.

Degree	ST	SDME-M	Ratio ST/SDME
2	68.37	9.99	6.84
4	172.19	7.97	21.60
6	297.48	16.48	18.05

Table 12: Average number of iterations for convergence using the conjugate gradient method with a GS preconditioner for the ST and SDME-M bases. We observe a very significant ratio, up to 21.6 using the SDME-M basis.

Degree	ST (s)	SDME-M (s)	Speedup
2	0.0153	0.0026	5.88
4	0.6279	0.0363	17.30
6	5.7101	0.3537	16.43

Table 13: Average time per time step using the conjugate gradient method with a GS preconditioner for the ST and SDME-M bases. We observe that the speedup obtained is similar to the ratio between the number of iterations.

Next, we present the same performance results using the element-by-element conjugate gradient solver with tolerance of 10^{-12} using a diagonal preconditioner, with results shown in Table 14. In this case, we used the optimization flag -O3 for compilation, which affects the total computational time, but not the number of iterations for convergence. The performance results in terms of speedup are presented in Table 15.

Degree	ST	SDME-M	Ratio ST/SDME
2	89.24	17.95	4.97
4	333.70	12.06	27.7
6	467.40	26.16	17.86

Table 14: Average number of iterations for convergence using the conjugate gradient method with a diagonal preconditioner for the ST and SDME-M bases.

Degree	ST (s)	SDME-M (s)	Speedup
2	0.0093	0.0053	1.75
4	0.3129	0.0408	7.67
6	2.2516	0.2905	7.75

Table 15: Average time per time step using the conjugate gradient method with a diagonal preconditioner for the ST and SDME-M bases.

5.3.2 Implicit time integration

For the implicit Newmark integration scheme, we first consider the following fabricated solution for $u(x,t)$:

$$u_x = X^4 \sin(2\pi t), \quad u_y = 0, \quad u_z = 0. \tag{58}$$

We considered the total time $T = 0.025\,s$ in this case, and therefore the solution gives $u_x = 0.157$ for $x = 1.0$ and $t = 0.025\,s$. The material properties and boundary conditions are the same as the previous tests. We considered the tolerance of 1×10^{-12} for the norm of the residual ψ in the Newton method.

We considered the spatial convergence analysis using a fixed $\Delta t = 3.90 \times 10^{-4}\,s$ and increasing the polynomial order. The convergence in time is analysed with fixed $P = 5$ and decreasing the time increments Δt. The results for both cases are shown in Fig.2.

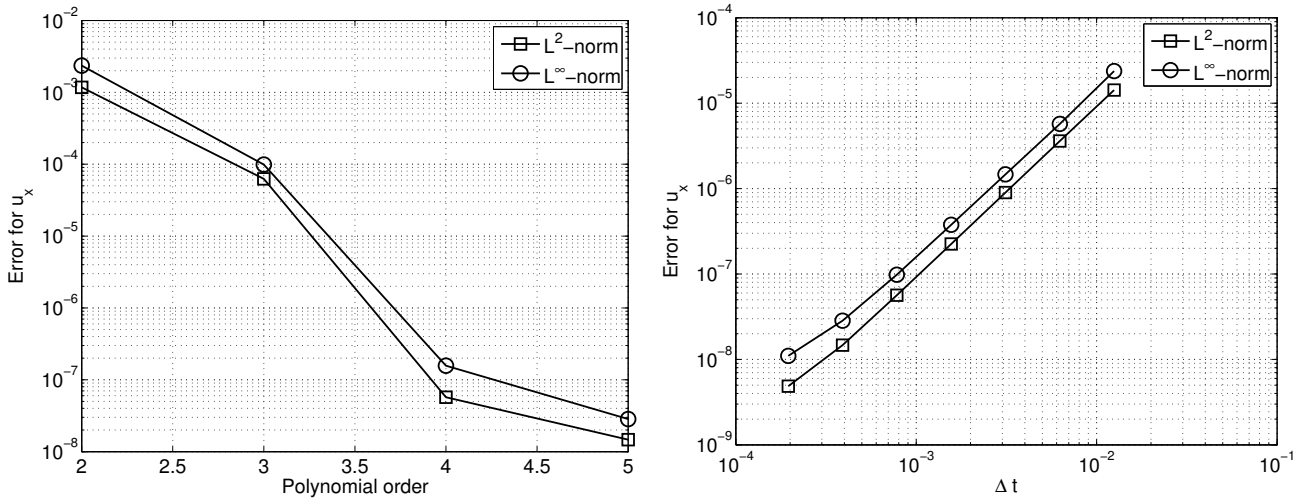

(a) Spatial convergence (b) Time convergence

Figure 2: Spatial convergence using $\Delta t = 3.90 \times 10^{-4}\, s$ and increasing the polynomial order P (a); Convergence in time with $P = 5$ and decreasing the time increment Δt (b).

We tested the performance of bases ST, SDME-M, SDME-H with $k = 0.5$ and $\lambda = 100$ in terms of the average number of iterations, average time and speedup. The results are presented in Figures 3 and 4. In these cases, we used a conjugate gradient solver with GS preconditioner. We observe that in general, the SDME-M performs better than the SDME-H basis, with a speedup up to 19 with polynomial order $P = 4$. Nevertheless, the SDME-H basis with the chosen parameters achieved at least a speedup ration of 3 compared to the ST basis, as illustrated in Fig. 4.

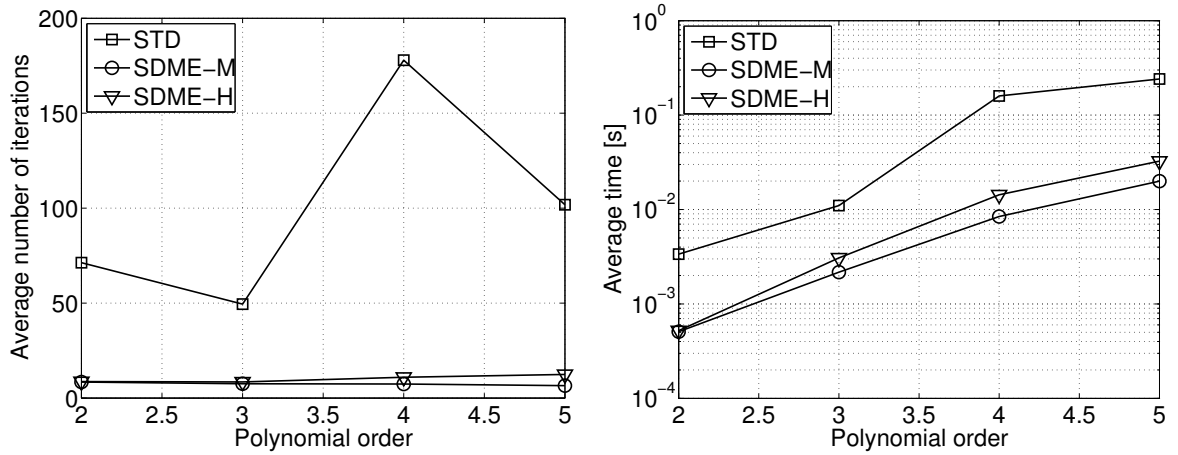

(a) Average number of iterations. (b) Average time.

Figure 3: Average number of iterations for linear system solution using CGGS in terms of the polynomial order, $\Delta t = 3.90 \times 10^{-4}\, s$ (a); Average time for linear system solution in terms of the polynomial order (b).

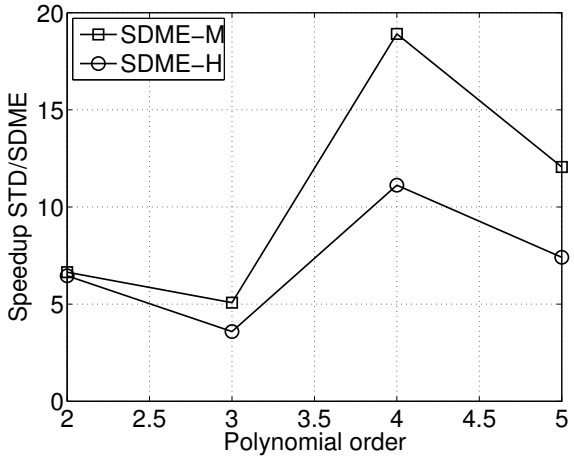

Figure 4: Speedup ratio for the computation time to solve the linear system of equations between the standard Jacobi basis and the minimum energy bases SDME-M, with $k = 0.5$, and SDME-H, with $k = 0.5$ and $\lambda = 100$.

We also considered the solution using the conjugate gradient solver with a diagonal preconditioner (CGD). The results are presented in Figures 5 and 6. We observe that similar to using a GS preconditioner, both minimum energy bases performed much better than the ST, with speedups up to 26 for the SDME-M basis. In general, the speedup achieved by the SDME-M basis was also higher than the SDME-H basis.

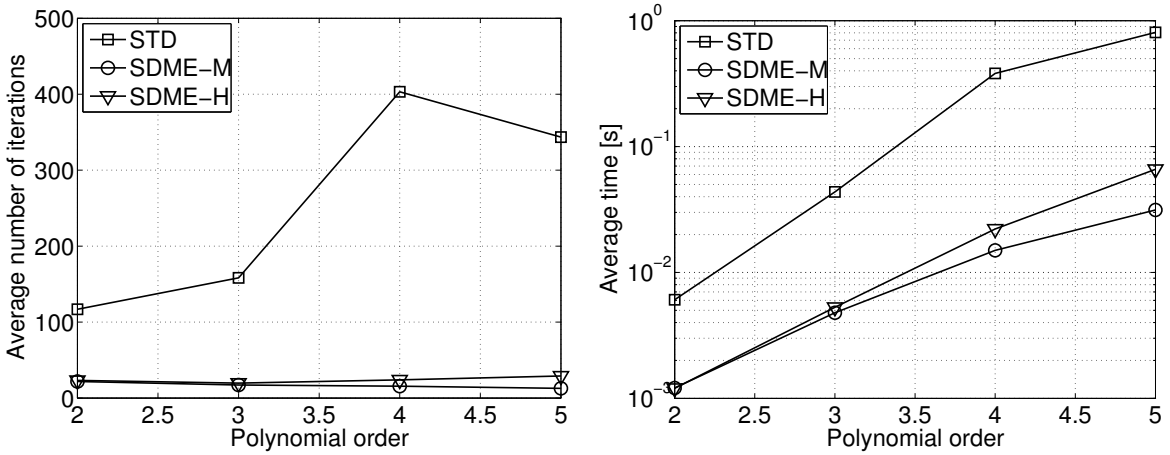

(a) Average number of iterations.

(b) Average time.

Figure 5: Average number os iterations for linear system solution using CGD in terms of the polynomial order, $\Delta t = 3.90 \times 10^{-4}\, s$ (a); Average time for linear system solution in terms of the polynomial order (b).

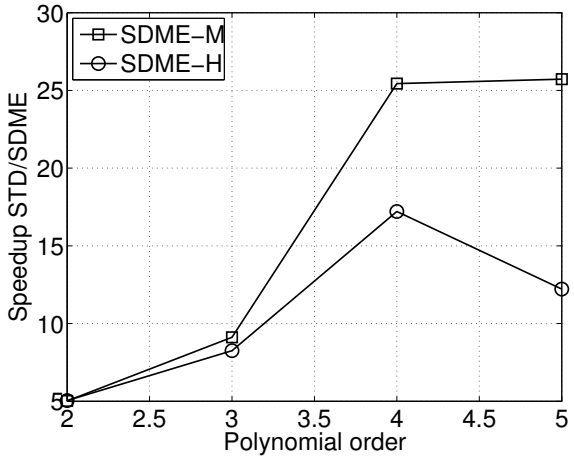

Figure 6: Speedup ratio for the computation time to solve the linear system of equations between the standard Jacobi basis and the minimum energy bases SDME-M, with $k = 0.5$, and SDME-H, with $k = 0.5\,\lambda = 100$.

The sinusoidal solution in space and time (Eq.55) was also considered. The results for convergence and performance of the bases are presented in Tables 16, 17 and 18. We observe that the performance for the SDME-H basis is slightly better than the SDME-M until degree $P = 4$. Beyond this polynomial degree, the SDME-M basis has a better performance.

5.3.3 Remark

We observe that the present results for the performance of the SDME bases with the Newmark scheme are distinct from those obtained for the linear transient problems solved in [8]. In the linear transient problem, the SDME-H basis performed better than the SDME-M basis for the implicit Newmark scheme. One possible reason for the observed results in this work is that the SDME-H basis was originally developed for the transient linear problem, which uses the same equivalent stiffness matrix $\left[\hat{K}\right]$ for the whole time integration, assuming constant time increments Δt. In that sense, the norm $\left[\alpha^H\right]$ used in the SDME-H basis had the same form as the operator of the problem. However, in the nonlinear case, the discrete operator contains a tangent stiffness matrix $[K_T]$ that constantly changes according to the kinematics of the simulation.

We would also like to notice that in the case of the static nonlinear problem, although the tangent stiffness matrix changes in every Newton iteration until convergence, the stiffness matrix is more similar to the tangent operator than the mass matrix is. This could explain the reason why the SDME-H basis had a better performance than the SDME-M basis.

Degree	Number of DOFs	L^2 error		
		u_x	u_y	u_z
2	276	2.09e-3	2.54e-4	2.35e-4
4	1246	3.40e-6	5.09e-7	5.54e-7
6	3084	9.17e-8	2.23e-8	2.22e-8

Table 16: L^2 error using Newmark integration, Schur complement, SDME-H basis, 8 hexahedra, $\Delta t = 2 \times 10^{-3}\,s$.

Degree	ST	SDME-M	SDME-H	Ratio ST/SDME-M	Ratio ST/SDME-H
2	119.65	21.40	20.86	5.59	5.74
4	352.05	19.45	17.94	18.10	19.62
6	610.83	32.28	42.01	18.92	14.54

Table 17: Average number of iterations for convergence using the conjugate gradient method with a diagonal preconditioner for the ST, SDME-M ($k = 0.5$), and SDME-H ($k = 0.5$, $\lambda = 100$) bases, Newmark integration, $\Delta t = 2 \times 10^{-3}\, s$. We observe a smaller number of iterations for the SDME-H basis until $P = 4$. The presented ratios are comparable to the results presented in Table 14, except for $P = 4$.

Degree	ST (s)	SDME-M (s)	SDME-H (s)	Speedup ST/SDME-M	Speedup ST/SDME-H
2	0.0066	0.0011	0.0012	6.000	5.500
4	0.3167	0.0185	0.0176	17.119	17.994
6	2.8062	0.1561	0.1963	17.977	14.295

Table 18: Average time per linear system solution using the conjugate gradient method with a diagonal preconditioner for the ST, SDME-M ($k = 0.5$), and SDME-H ($k = 0.5$, $\lambda = 100$) bases, Newmark integration, $\Delta t = 2 \times 10^{-3}\, s$. The speedup is higher than the results presented in Table 15, but in this case we are only measuring the time for linear system solution instead of the entire time step.

Authors are the only responsible for the printed material included in this paper.

6. CONCLUSIONS

In this work we applied high-order finite element bases to solve transient, nonlinear elastic structural problems in 2D and 3D. The bases were constructed by performing a simultaneous diagonalization of the internal modes and Schur complement of the boundary modes in the 1D basis. The multi-dimensional operators were constructed with tensor products of the one-dimensional mass and linear stiffness matrices. Fabricated smooth solutions involving large displacements and strains were used to test the bases in static and transient (explicit and implicit) formulations. From the obtained results, we observed that:

- The SDME bases performed significantly better than the standard Jacobi basis for all nonlinear problems tested (static, transient with explicit and implicit time integration).
- For the static nonlinear tests, the SDME-H basis had a better performance than the SDME-M basis for all polynomial orders when using a Gauss-Seidel preconditioner for linear system solution. The same was observed when using the diagonal preconditioner until $P = 6$.
- In the case of transient nonlinear problems, with explicit time integration, the SDME-M basis had a speedup up to 27.7 when compared to the standard Jacobi basis.
- For the implicit time integration, the best results for speedup were achieved by the SDME-M basis as well, with speedup up to 26.
- The use of the 1D matrices procedure obtained a speedup of 2 compared to the standard calculation procedure, for 2D and 3D tangent stiffness matrices. We observe that this speedup is relevant, since the calculation of high-order matrices at every Newton iteration for every time step is a costly process.

7. ACKNOWLEDGEMENTS

Authors would like to thank the São Paulo Research Foundation (FAPESP) under grants 2013/50238-3 and 2012/19922-2, the Coordination for the Improvement of Higher Education Personnel (CAPES) under grant 33003017, and also the National Council for Research and Development (CNPq) under grant 306182/2014-9.

REFERENCES

[1] Karniadakis, G. E. and Sherwin, S. J. (2005). Spectral/hp Element Methods for Computational Fluid Dynamics. Oxford University Press, Oxford.

[2] Bittencourt, M. (2014). Computational solid mechanics: variational formulation and high order approximation. CRC Press, 1st edition.

[3] Babuska, I., Szabó, B. A., and Katz, I. N. (1981). "The p-version of the finite element method." SIAM J. Numer. Anal., 18(3):515–545.

[4] Carnevali, P., Morris, R. B., Tsuji, Y., and Taylor, G. (1993). "New basis functions and computational procedures for *p*-version finite element analysis." International Journal for Numerical Methods in Engineering, 36:3759–3779.

[5] Bittencourt, M. L., Vazquez, M. G., and Vazquez, T. G. (2007). "Construction of shape functions for the *h*- and *p*-versions of the FEM using tensorial product." International Journal for Numerical Methods in Engineering, 71:529–563.

[6] Nogueira Jr, A. C. and Bittencourt, M. L. (2007). "Spectral/HP finite elements applied to linear and non-linear structural elastic problems." Latin American Journal of Solids and Structures, 4(1):61–85.

[7] Dong, S. and Yosibash, Z. (2009). "A parallel spectral element method for dynamic three-dimensional nonlinear elasticity problems." Computers and Structures, 87:59–72.

[8] Rodrigues, C., Suzuki, J., and Bittencourt, M. (2016). "Construction of minimum energy high-order Helmholtz bases for structured elements." Journal of Computational Physics, 306:269–290.

[9] Shen, J. and Wang, L.-L. (2007). "Fourierization of the Legendre–Galerkin method and a new space–time spectral method." Applied numerical mathematics, 57(5):710–720.

[10] Šolín, P. and Vejchodskỳ, T. (2008). "Higher-order finite elements based on generalized eigenfunctions of the Laplacian." International journal for numerical methods in engineering, 73(10):1374–1394.